NJC

PAPER

View Article Online
View Journal | View Issue

Cite this: *New J. Chem.*, 2025, **49**, 15434

Improving excited-state dynamic properties with the help of metalide character and excess electrons: earlier transition-metal pairing with superalkali clusters

Atazaz Ahsin,[ac] Aamna Qamar,[bc] Sadegh Kaviani,[d] Safi Ullah Majid,[e] Jianwei Cao *[a] and Wensheng Bian *[ac]

Recognizing the increased stability of metalide complexes over alkali anions, research on transition metal-based metalides continues to grow. Here, employing various quantum chemical methods, we investigate novel superalkali-M (where M = Sc, Ti, V, Cr, and Mn) pairings theoretically, and our results indicate that the excited-state dynamic properties of these complexes are enhanced due to their metalide character and excess electrons. In the designed Li_3O@[12-crown-4]M complexes, Li_3O demonstrates excellent charge transfer through van der Waals (vdW) interactions. *Ab initio* molecular dynamic simulations demonstrate their kinetic and dynamic stabilities, and the thermodynamics of physisorption is also unveiled. A remarkable hyperpolarizability value of 7.6×10^5 a.u. is observed for the Sc complex, while the hyper-Rayleigh scattering value is highest for the Mn complex. The influence of different solvents on the hyperpolarizability response is thoroughly investigated. Moreover, dynamic NLO parameters are computed using various externally applied frequencies. The nature of bonding and the role of vdW interactions in triggering NLO responses are unveiled. In addition to the infrared analysis, the effect of vertical excitation energy has also been investigated in enhancing dynamic NLO features. We hope that these findings hold promise for advancing NLO applications of organic functional materials.

Received 24th February 2025,
Accepted 3rd August 2025

DOI: 10.1039/d5nj00827a

rsc.li/njc

1 Introduction

Solvated electrons (excess electrons) are fundamental entities in numerous fields of physical science due to their emerging demands in atmospheric chemistry, reduction reactions, and nonlinear optics.[1–3] In 1916, Gibson and Argo demonstrated the interaction of ammonia with alkali metals, revealing intriguing optical and absorption properties.[4] After the discovery and exploration of excess electron compounds, the term ''solvated electrons'' was coined to describe such species. Inspired by solvated electrons, Dye's group synthesized the first excess electron compound (Cs^+(18-crown-6)$2e^-$) in 1983, which exhibits electride character.[5] The excess electrons in molecules and compounds occupy diffuse Rydberg orbitals (loosely held), imparting extraordinary features to them.[6] Recent advancements underscore the compelling properties of excess electron compounds in catalysis, optics, and electrode materials.[9,10] Additionally, various organic and inorganic complexes have been recognized as excess electron compounds.[3,7] In the last two decades, a series of reports have uncovered the dramatic role of loosely bound electrons in regulating the hyperpolarizability of various molecules.[7,8,11,12] The presence of excess electrons predominately reduces the excitation energy (ΔE) during electron excitation (from the HOMO to the LUMO), resulting in an appreciable enhancement in the hyperpolarizability of molecules.

Alkalides containing alkali metal anions (*e.g.*, Li^-, Na^-, K^-, and Cs^-) and electrides housing trapped electrons (anions) intercalated within an organic complexant are exemplary representatives of the excess electron family. Alkalides can be used as excellent nonlinear optical (NLO) materials[9] and offer a significantly narrow band gap for condensed matter physics.[10] Various conventional alkalides based on single alkali

---

[a] *Beijing National Laboratory for Molecular Sciences, Institute of Chemistry, Chinese Academy of Sciences, Beijing 100190, China. E-mail: caojw@iccas.ac.cn, bian@iccas.ac.cn*
[b] *Beijing National Laboratory for Molecular Sciences, State Key Laboratory of Polymer Physics and Chemistry, Chinese Academy of Sciences, Beijing 100190, China*
[c] *School of Chemical Sciences, University of Chinese Academy of Sciences, Beijing 100049, China*
[d] *Institute of Physics, Kazan Federal University, 420008 Kazan, Russia*
[e] *Department of Chemistry, Abbottabad Campus, COMSATS University Islamabad, Abbottabad 22060, KPK, Pakistan*

metals have been documented in the literature.[12–17] On the other hand, non-traditional alkalides containing coinage metals (Cu, Ag, and Au),[11] superalkali (Li_3O)-based alkalides,[12] and alkaline earth metal-based earthides (Be, Mg, and Ca) have been investigated and were grouped into excess electron compounds. However, substituting alkali metals with more stable d-block metals or clusters of atoms is a promising strategy for achieving thermodynamically stable complexes.[12,13,20–23] For instance, Sun *et al.*[11] proposed using coinage metals to design metalides (transition metal as an anion) as alternatives to alkali anions. Due to the higher ionization potential of coinage metals compared to alkali, the proposed metalide complexes have good thermodynamic and electronic stability. Doping of transition metals (particularly those in the 3d series) is expected to be a promising strategy for designing complexes with metalide character.[15–21]

For designing metalide and alkalide complexes, superalkali clusters are potential candidates.[22] For example, a significant charge transfer in superalkali-M (where M = Li, Na, and K) pairing was observed from superalkali clusters to alkali metals, demonstrating alkalide characteristics.[22] Superalkali clusters, such as Li_3O, have lower ionization potentials (IPs) than alkali metals[23,24] and strong reduction potential, making them intriguing substitutes for alkali metals in constructing alkalide or metalide complexes. In particular, Li_3O stands out as an experimentally validated system with distinctive electronic properties and remarkably low ionization energy. Obviously, superalkali clusters very actively display electropositive properties and non-covalent interactions, promoting the physiochemical properties of the obtained complexes.[12] Furthermore, it is known that the formation and stabilization of metalide complexes require stringent chemical environments and involve either a disproportionation or the reduction of one elemental metal by another metal or cluster of atoms.[25] Generally, the reduction process and charge transfer are facilitated by strong stabilization of the metal cation by complexants such as crown ethers and cryptands.[26] Crown ethers are heterocyclic polyethers capable of forming host–guest complexes, especially from the atomic scale to large molecular clusters.[27,28] To our knowledge, the exploration of superalkali–transition metal pairing using [12-crown-4] has not yet been undertaken for optical and NLO applications. Although conventional metalides, based on single metal doping on complexes, have been reported,[13,20,21] the effect on charge transfer in long-range interactions using superalkali–transition metal pairing would improve the stability of metalides and thus be a good choice for designing molecular functional materials.[22,29] In addition, van der Waals (vdW) interactions are very important in many chemical systems and reactions,[30–35] making it necessary to investigate the role of vdW interactions in the present designed complexes.

In this work, we present a detailed theoretical study on Li_3O–M (M = Sc, Ti, V, Cr, and Mn) pairing on both sides of [12-crown-4]. In contrast to traditional alkalides and metalides based on single metals, a significant metalide characteristic has been observed in Li_3O@[12-crown-4]M complexes. The designed metalide complexes show excellent charge transfer between Li_3O and M, which is crucial for boosting NLO properties. The excited-state dynamic properties of these complexes are improved with the help of metalide character and excess electrons. The formation and stability of these complexes are also investigated *via* molecular dynamics calculations, and the important role of vdW interactions is underscored in triggering NLO features.

2 Computational details

All quantum chemical simulations were carried out using the Gaussian 16 package,[36] while molecular dynamics simulations were performed using the ORCA 5.0 program.[37] To make the results reliable, the method and basis set should be carefully chosen.[38–42] The molecular geometries for the designed Li_3O@[12-crown-4]M (M = Sc, Ti, V, Cr, and Mn) complexes were determined using the artificial bee colony (ABC) algorithm as implemented in the ABCluster program,[43,44] which was connected with the Gaussian 16 package. In the ABCluster program, 500 initial guess structures were auto-generated by randomly sampling and perturbing atomic coordinates, whose single-point energy was then evaluated at the semiempirical PM6 level. 100 lowest-energy structures were selected for further optimization at the ωB97xd/def2-tzvp level. This method was validated to yield reliable results through comparisons with various hybrid DFT methods (Table S1) and our previous studies.[40,43] Besides, spin multiplicities were analyzed, considering only low-energy states for further simulations. The entire optimization and frequency calculations were performed at the same level (ωB97xd/def2-tzvp) without any symmetry constraints. The stability of wavefunction was verified before proceeding with further simulations.

Energetics of complexes were investigated by computing several parameters, such as the interaction energy (ΔE_{int}), Gibbs free energy of formation (ΔG_f), adsorption enthalpy (ΔH), and adsorption entropy (ΔS) at 1 atm and 298.15 K. In particular, the complex formation strength is validated by computing ΔE_{int}, which was computed using the following equations:

$$\Delta E_{\text{int}} = E_{\text{Li}_3\text{O@[12-crown-4]M}} - \left(E_{\text{[12-crown-4]}} + E_{\text{Li}_3\text{O}} + E_{\text{M}}\right) \quad (1)$$

where $E_{\text{Li}_3\text{O@[12-crown-4]M}}$ is the energy of the optimized complex. $E_{\text{[12-crown-4]}}$, $E_{\text{Li}_3\text{O}}$, and E_{M} represent the energy of the crown ether, superalkali and the transition metal, respectively. ΔE_{int} was then corrected for basis set superposition error (BSSE) through the counterpoise approach[45] by

$$\Delta E^{\text{CP}}_{\text{int}} = \Delta E_{\text{int}} + \text{BSSE} \quad (2)$$

where $\Delta E^{\text{CP}}_{\text{int}}$ denotes the BSSE-corrected interaction energy. Likewise, the obtained thermodynamic properties are given by the following expressions:

$$\Delta G = G_{\text{Li}_3\text{O@[12-crown-4]M}} - \left(G_{\text{[12-crown-4]}} + G_{\text{Li}_3\text{O}} + G_{\text{M}}\right) \quad (3)$$

$$\Delta H = H_{\text{Li}_3\text{O@[12-crown-4]M}} - \left(H_{\text{[12-crown-4]}} + H_{\text{Li}_3\text{O}} + H_{\text{M}}\right) \quad (4)$$

$$\Delta S = \frac{\Delta H - \Delta G}{T} \tag{5}$$

To further understand the electronic properties and superalkali-like nature of the designed complexes, the vertical ionization potential (VIP) and vertical electron affinity (VEA) were calculated using the following equations:

$$\mathrm{VIP} = (E)^+ - (E)^0 \tag{6}$$

$$\mathrm{VEA} = (E)^- - (E)^0 \tag{7}$$

Here, $(E)^0$ represents the energy of the neutral structure, whereas $(E)^+$ and $(E)^-$ are the energies of cationic and anionic structures, respectively.

To analyse the simultaneous interaction of Li_3O and M on [12-crown-4] and the kinetic stability of complexes, *ab initio* molecular dynamics (AIMD) simulations were conducted using the ORCA 5.0 package.[37] Due to the high computational cost for AIMD simulation at the ωB97xd/def2-tzvp level, the simulations were performed at the B3LYP-D3/def2-SVP level of theory,[46] with the optimized geometry at the ωB97xd/def2-tzvp level used as the initial geometry. In AIMD simulations, each trajectory was simulated for 750 fs with a step size of 0.5 fs at 298.15 K. Furthermore, the metalide character of the Li_3O@[12-crown-4]M complexes and charge transfer were explored using the frontier molecular orbital (FMO), natural bond orbital (NBO), electron localizing function (ELF), and localized orbital locator (LOL) analyses. Charge decomposition analysis (CDA) is also exploited using the same method to determine charge donation (Li_3O → TM) and back donation (TM → Li_3O) in present complexes. To determine the static NLO characteristics, the dipole moment (μ_o), polarizability (α_o), first-order hyperpolarizability (β_o), static second hyperpolarizability (γ_o), and scattering hyperpolarizability (β_{HRS}) were calculated using the following equations:

$$\mu_o = (\mu_x^2 + \mu_y^2 + \mu_z^2)^{\frac{1}{2}} \tag{8}$$

$$\alpha_o = 1/3(\alpha_{xx} + \alpha_{yy} + \alpha_{zz}) \tag{9}$$

$$\beta_o = \sqrt{\beta_x^2 + \beta_y^2 + \beta_z^2} \tag{10}$$

where

$$\beta_x = \beta_{xxx} + \beta_{xyy} + \beta_{xzz},\ \beta_y = \beta_{yyy} + \beta_{yzz} + \beta_{yxx} \text{ and } \beta_z = \beta_{zzz} + \beta_{zxx} + \beta_{zyy}$$

$$\langle\gamma\rangle = 1/5(\gamma_{xxxx} + \gamma_{yyyy} + \gamma_{zzzz} + \gamma_{xxyy} + \gamma_{xxzz} + \gamma_{yyxx} + \gamma_{yyzz} + \gamma_{zzxx}) \tag{11}$$

Here, β_{ijk} $(i, j, k = \{x, y, z\})$ is the tensor component of β_o and γ_{ijkl} $(i, j, k, l = \{x, y, z\})$ is the tensor component of second hyperpolarizability (γ_o). The second hyperpolarizability (γ) is the fourth rank tensor of 3 × 3 × 3 × 3 form, which exhibits both static and dynamic nature,

$$\beta_{HRS}(-2\omega;\omega,\omega) = \sqrt{\langle\beta_{zzz}^2\rangle + \langle\beta_{zxx}^2\rangle} \tag{12}$$

where $\langle\beta_{zzz}^2\rangle$ and $\langle\beta_{zxx}^2\rangle$ are the averages of the orientational (β) tensor. The related depolarization ratio (DR) is calculated as follows:

$$\mathrm{DR} = \langle\beta_{zzz}^2\rangle/\langle\beta_{zxx}^2\rangle \tag{13}$$

In addition, the implicit solvation model based on density (SMD) has been considered to examine the effect of dielectric constants and protic solvent nature on hyperpolarizability response, with water, ethanol and *N*,*N*-dimethylformamide (DMF) considered.

Frequency-dependent (dynamic) nonlinear optical parameters were calculated at 532, 1064, 1300, and 1500 nm. Frequency-dependent first hyperpolarizability electro-optic Pockel's effects $\beta_{EOPE}(\omega) = \beta(-\omega;\omega,0)$ and $\beta_{ESHG}(\omega) = \beta(-2\omega;\omega,\omega)$ were obtained. The second hyperpolarizability $\gamma(\omega)$, dc-Kerr $\gamma_{\text{dc-Kerr}}(\omega) = \gamma(-\omega;\omega,0,0)$ and second harmonic generation $\gamma_{ESHG}(\omega) = \gamma(-2\omega;\omega,\omega,0)$ were also calculated similarly. Excited state studies were conducted by considering the time-dependent density functional theory (TD-DFT) approach at the same level of theory. In the present study, 60 electronic states were considered, including both singlets and triplets in determining the excited state parameters and absorbance wavelengths. To observe changes in vibrational modes after doping Li_3O and M, we compared the vibrational frequency of complexes and pristine [12-crown-4] at the ωB97xd/def2-tzvp level. Furthermore, total density of states (TDOS) and projected density of states (PDOS) studies were conducted to unveil the orbital contribution and electrical properties of complexes.[47]

The topological features of complexes were analysed through non-covalent interaction (NCI) and quantum theory of atoms in molecules (QTAIM) analyses as implemented in Multiwfn[48] and visual molecular dynamics (VMD) program.[49] The NCI index relies primarily on the reduced density gradient (RDG) and electron density (ρ), and their correlation can be described using the equation given below:

$$\mathrm{RDG} = \frac{1}{2(3\pi)^{1/3}}\frac{\nabla^2\rho}{\rho^{3/4}} \tag{14}$$

The stabilization energy (E^2) during the electron delocalization between the donor (i) and acceptor (j) interacting orbitals was estimated through the NBO analysis. The following equation was used to calculate the E^2 of the present complexes:

$$E^2 = \Delta E_{i,j} = -q_i\frac{F_{(i,j)}{}^2}{E_j - E_i} \tag{15}$$

Here, $F_{i,j}$ is the off-diagonal NBO Fock matrix element and q_i is the donor orbital occupancy. E_i and E_j are the diagonal elements (orbital energies).

3 Results and discussion

3.1 Electronic structure and thermodynamic stability

We initiated our investigation on the electronic structure of Li_3O@[12-crown-4]M complexes by employing quantum chemical and molecular dynamic simulations. Transition metal complexes can exhibit different spin multiplicities depending on the distribution of electrons in 3d orbitals, which can influence their physical and chemical properties. Earlier transition metals are often intrinsically highly reactive as a result of their strong reducing power and increasing oxidation state. The most stable spin states of the present complexes are presented in Table 1. As can be seen, the highest stable spin (septet) multiplicity corresponds to the Mn complex. Fig. 1 depicts the important 2D and 3D visualization of Li_3O, [12-crown-4], M, and complex structures, while optimized molecular geometries of complexes are shown in Fig. S1. Only the important interaction distances are considered in the present complexes. The Li_3O cluster exhibits a highly symmetric triangular structure, where the calculated Li–O bond length (1.67 Å) and the Li–O–Li bond angle (120°) are consistent with those in a previously reported study.[50] A slight deviation in the Li–O bond length and the Li–O–Li angle is observed after its vertical adsorption on [12-crown-4]. Similarly, the calculated average bond length of C–O in [12-crown-4] is 1.40 Å and other bond distances are also comparable to experimental values. The Li_3O cluster contains 9-valence electrons, 6 from oxygen and 3 from lithium, and the nature of the cluster mimics the chemistry of individual alkali metals. Hence, after losing one electron, it achieves a close shell electronic configuration, $1s^2 2p^6$. Therefore, simultaneous interactions of Li_3O and M with [12-crown-4] would result in metalide nature in complexes with unique optical and NLO features. The binding distance of M with oxygen atoms of [12-crown-4] (d_{M-O}) and the distance between the Li-atom and oxygen atoms (d_{Li-O}) are computed (Table 1). Likewise, the distance of lower M with the H-atom of [12-crown-4] (d_{M-H}) is also determined. The d_{M-O} in entire complexes ranged between 3.59 and 5.58 Å, with no significant elongation in the Li–O bond. Despite the slight structure distortion, the distance of O–Li manifests the chemical bond between oxygen and Li atoms, demonstrating that Li_3O retains its integrity during the interaction with [12-crown-4]. The optimized geometry coordinates of complexes are provided in Table S2. Further illustrations of geometric parameters are discussed in the SI (Section S1). The interaction distance of the M metal with the complexant steadily rises from Sc to Mn, which can be correlated with high nuclear charge and spin multiplicities in comparison to Sc- and Ti-based complexes. The longer metal–oxygen bond distance (d_{M-O}) in the Mn complex arises from the electronic stability conferred by its half-filled d-orbital configuration, which reduces Jahn–Teller distortions compared to the Sc, Ti, and V complexes. Overall, the trend of d_{M-O} in the present complexes is Sc < Ti < V < Cr < Mn.

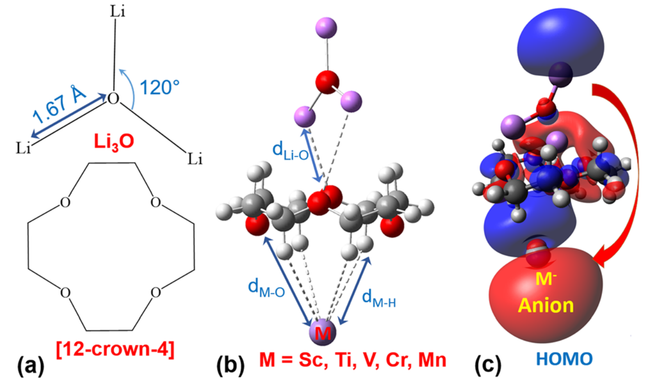

Fig. 1 2D and 3D representation of molecular geometries of individual molecules and the present complexes: (a) 2D molecular structure of Li_3O and [12-crown-4], (b) 3D molecular representation of Li_3O@[12-crown-4]M during complex formation, and (c) occupied molecular orbital of the complex (isovalue = 0.025) at the B3LYP-D3/def2tzvp level. The red and pink colors represent oxygen and lithium atoms, respectively.

We can also see from Table 1 that the values of ΔE_{int} and ΔE_{int}^{CP} are lower than 23 kcal mol^{-1}, indicating the physical interactions between the three components during complex formation.[30] The much negative ΔE_{int} (also see Table S1) justifies a strong complexation among three components of present complexes. Our computed interaction energies are slightly smaller than those reported for coinage-based metalides Cu–$F_6C_6H_6$–Cu and Cu–$F_6C_6H_6$–Ag.[11] The strong binding of anions and cations with $F_6C_6H_6$ could be the reason for their increased interaction energy. However, in the case of single alkali metal-based metalides Li–$F_6C_6H_6$–Sc and Na–$F_6C_6H_6$–Sc, and K–$F_6C_6H_6$–Sc,[20] the interaction energies of present complexes are significantly high, signifying the strong complexation of Li_3O with transition metals. Hence, Li_3O pairing with transition metals might be a better strategy for enhancing dynamic NLO features in the present complexes.

Table 1 also presents thermodynamic parameters, in which the thermodynamic feasibility and spontaneity of complex formation can be evidenced by the negative change in ΔG_f of formation ($\Delta G < 0$). A $\Delta G_{298.15}$ value of −21.35 kcal mol^{-1} is obtained for the Sc complex, indicating exothermic adsorption processes, which also agrees with its strong interaction energy.

Table 1 Calculated interaction bond distances (*d*), interaction energies (ΔE_{int}), BSSE-corrected interaction energies (ΔE_{int}^{CP}), Gibbs free energy of formation (ΔG_f), adsorption enthalpy (ΔH), and adsorption entropy (ΔS) of the Li_3O@[12-crown-4]M complexes

			Interaction distances			Energies				
Complexes	Symmetry	Spin	d_{M-H} (Å)	d_{M-O} (Å)	d_{Li-O} (Å)	ΔE_{int} kcal mol^{-1}	ΔE_{int}^{CP} kcal mol^{-1}	ΔG_f kcal mol^{-1}	ΔH kcal mol^{-1}	ΔS kcal (mol K)$^{-1}$
Li_3O@[12-crown-4]Sc	C_1	Triplet	3.23	3.59	2.52	−48.74	−34.93	−26.09	−44.47	−0.06
Li_3O@[12-crown-4]Ti	C_1	Doublet	3.31	4.01	2.54	−86.97	−41.95	−64.61	−82.66	−0.06
Li_3O@[12-crown-4]V	C_1	Quintet	3.43	4.80	2.54	−98.25	−98.36	−68.12	−93.69	−0.08
Li_3O@[12-crown-4]Cr	C_1	Sixet	3.25	4.91	2.60	−197.98	−149.86	−178.12	−193.50	−0.05
Li_3O@[12-crown-4]Mn	C_1	Septet	3.34	5.58	2.55	−131.39	−114.75	−72.51	−90.43	−0.06

The feasibility of complex formation decreases progressively from the Sc to Mn complexes (with increased atomic number). This is reasonable since the increase of the number of d-electrons from Sc to Mn in the 3d-series leads to strong binding and less distortion due to the moderate interaction distance ($d_{\mathrm{M-O}}$). Excellent correlation is observed between the thermodynamic parameters (ΔG and ΔH) and the computed interaction energies. A similar pattern of reduction in $\Delta H_{298.15}$ can also be observed in Table 1.

The AIMD approach is reliable and versatile to unveil the thermodynamic and kinetic stability of molecular complexes at the atomic scale, offering significantly reduced computational costs relative to quantum dynamics simulations.[51–54] In the obtained 1500 distinct geometries associated with the trajectory of the complex, no dissociation or fragmentation pattern is observed, indicating the stability of complex formation (adsorption) and thermodynamic stability at room temperature. The calculated root-mean-square deviation (RMSD) and kinetic energy are shown in Fig. 2. As can be seen from Fig. 2a, the root-mean-square distances increase up to 1.0 Å, and equilibrium during simulations is attained after 500 fs except for [12-crown-4], which relaxes after 600 fs. Although RMSD values increase in the beginning, no distortion in complexes is observed. The fluctuations are higher for Sc and Ti complexes, but decrease for V to Mn complexes. This can be correlated with nuclear charge and variable spin multiplicities of 3d-transition metals in complexes. The higher interaction energy of Cr and Mn complexes is consistent with its reduced RMSD trend, probing the relatively high dynamic stability among complexes. Also, a small fluctuation in the RMSD curve for Cr and Mn complexes might be correlated with strong binding of M having less distortion effect with [12-crown-4]. An increasing trend in total kinetic energy has been recorded up to 200 fs, where equilibrium is achieved after 300 fs. The snapshots of geometries during AIMD simulations are provided in Fig. S2. The conformations of each complex were taken after every 300 fs to ensure structural integrity during AIMD simulations.

3.2 Metalide character and excess electron nature

The natural bonding orbital (NBO) and Mulliken's atomic charges are computed for Li_3O and M in the present Li_3O@[12-crown-4]M complexes. Strong metalide character (Sc^-, Ti^-, V^-, Cr^-, and Mn^-) has been confirmed through various quantum chemical calculations. A significant charge transfer is recognized to transition metals from the Li_3O cluster, indicating the superalkali-metalide ionic pairings ($Li_3O^{\&+}\cdots M^{\&-}$). Based on the results in Table 2, the computed NBO charges on M (QM) are negative and range from −0.23 to −0.93 |*e*|. The significant negative charge on transition metals ($Q_{\mathrm{M-}}$) and positive charge on $Li_3O^{\&+}$ suggest excellent metalide character. The metalide character in present complexes is more prominent as compared to conventional metalide complexes based on a single metal. The calculated NBO charges on Sc in the Li_3O@[12-crown-4]Sc complex are more negative as compared to those reported for $Li–F_6C_6H_6–Sc$.[20] In $Li–F_6C_6H_6–Sc$, Li does not provide the same degree of electron donating stabilization. The Li_3O cluster contains three electropositive Li atoms with a partially filled orbital ($2s^1$). The substantial electron delocalization in Li_3O, combined with its excellent electron-donating ability, generates a highly polar environment that increases the charge transfer capacity. Additionally, the sum of charges (Q_{sum}) on Li atoms in Li_3O range from 0.18 to 0.92 |*e*|, with the values being positive in magnitude, indicating a significant charge transfer from Li_3O to M. It is also evident that the Sc metal exhibits the highest negative charge (−0.93 |*e*|) among the other transition metals in the present complexes. Due to the involvement of the Li_3O in displaying metalide character, these complexes may be termed super-metalides or superalkali-based metalides. Based on these findings, the order of metalide character for the studied complexes is Li_3O^+@[12-crown-4]Sc^- > Li_3O^+@[12-crown-4]Ti^- > Li_3O^+@[12-crown-4]V^- > Li_3O^+@[12-crown-4]Cr^- > Li_3O^+@[12-crown-4]Mn^-. The high d-orbital occupancy and the stable d^5 configuration in Mn can indeed contribute to a smaller negative (anionic) NBO charge on Mn in the Li_3O@[12-crown-4]Mn complex. This half-filled configuration minimizes charge separation, as Mn retains greater electron density localized within its d-orbitals. The extended interaction distance between Mn and O in the Mn complex can further reduce its metalide character.

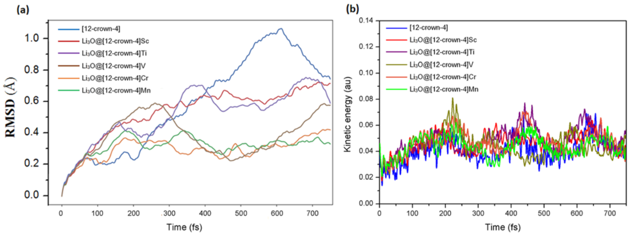

Fig. 2 (a) Root-mean-square deviation (RMSD) and (b) kinetic energy change with respect to time during the AIMD study of the [12-crown-4] and Li_3O@[12-crown-4]M complexes at the B3LYP-D3/def2-SVP level.

Furthermore, the charge decomposition analysis (CDA) offers comprehensive insights into charge transfer and bonding interactions within the Li_3O@[12-crown-4]M complexes by evaluating the primary contributions from the fragments ([12-crown-4], Li_3O, and M) involved in charge transfer. Notably, a substantial charge transfer is observed from Li_3O to M. Thus, the analysis focuses on the electron density contributions for donation ($Li_3O \rightarrow M$) and back donation ($M \rightarrow Li_3O$), which are summarized in Table S5. The findings correlate well with the aforementioned charge analysis (NBO) of the complexes, suggesting that the most prominent electron transfer occurs in the Li_3O@[12-crown-4]Sc complex, which exhibits a value of 0.44 |*e*|. A similar trend of charge donation was observed in Li_3O@[12-crown-4]Ti and Li_3O@[12-crown-4]Mn complexes. However, the charge donation ($Li_3O \rightarrow M$) is slightly reduced in Li_3O@[12-crown-4]V and Li_3O@[12-crown-4]Cr complexes. The negative NBO charge on M decreases from Sc to Mn, which is also consistent with charge donation ($Li_3O \rightarrow M$) in CDA analysis. Furthermore, the negative repulsive polarization (*r*)

Table 2 NBO charge on transition metals (Q_M, in |e|), sum of total positive charges on Li_3O (Q_{sum}, in |e|), Mulliken's atomic charge on transition metals (Q_{MM}, in |e|), HOMO energy (E_{HOMO}, in eV), LUMO energy (E_{LUMO}, in eV), energy gap (E_g, in eV), dipole moment (μ_o, in D), vertical ionization potential (VIP, in eV), and vertical electron affinity (VEA, in eV) of the complexes

Complexes	Q_M	Q_{Li}	Q_{sum}	Q_{MM}	E_{HOMO}	E_{LUMO}	E_g	μ_o	VIP	VEA
Li_3O	—	0.45	—	—	−7.17	−0.14	7.03	0	5.14	4.44
[12-crown-4]	—	—	—	—	−8.74	−3.06	5.68	0.84	5.72	4.25
Li_3O@[12-crown-4]Sc	−0.93	0.71	0.18	−0.22	−3.61	−0.31	3.30	5.19	0.27	3.48
Li_3O@[12-crown-4]Ti	−0.35	0.92	0.92	−0.20	−3.71	−0.88	2.83	5.70	1.09	1.36
Li_3O@[12-crown-4]V	−0.23	0.96	0.92	−0.82	−3.03	−0.35	2.68	19.24	2.45	1.18
Li_3O@[12-crown-4]Cr	−0.10	0.93	0.91	−0.87	−2.49	−0.59	1.90	18.55	3.27	0.82
Li_3O@[12-crown-4]Mn	−0.01	0.94	0.90	−0.02	−2.67	−1.03	1.64	10.10	4.08	0.35

observed in all complexes indicates a high charge density localized in the interaction region.

To further support the metalide character and excess electron nature, frontier molecular orbital (FMO) results are illustrated in Fig. 3. As can be seen, the highest occupied molecular orbital (HOMO) on the transition metals depicts the excess electronic cloud, indicating the negative NPA charges on transition metals. The HOMO and HOMO−1 densities have distribution across metal sites and on Li_3O. This distribution suggests that excess electrons are available to participate in charge driven optical properties. HOMOs are similar to s-orbitals except for the V complex, which represents the d-orbital shape, while the LUMO varies in shape from d_{xy} to d_{z^2}. The LUMOs of the V and Mn complexes have a shape similar to the d_{z^2} orbital. The electron in HOMO of the Ti complex is associated with the d_{xy} orbital, and the LUMO shape is reminiscent of the diffused s-orbital. On the other hand, molecular materials with significantly reduced HOMO–LUMO gaps (E_g) are highly desirable due to their potential optical and electrical properties. The [12-crown-4] has an E_g of 5.68 eV. The complexation of Li_3O with M reduced the E_g of the resulting complexes, indicating the strong interactions through vdW forces. After simultaneous adsorption of M and Li_3O on the complexant, a significant reduction in E_g values is observed, ranging from 1.64 to 3.30 eV (see Table 2). Among the complexes, the lowest E_g (1.64 eV) is observed for the Mn complex, while the highest one (3.30 eV) is found in the Sc complex. As shown in Table 2, the E_g decreases with the increased atomic number of M, which could be attributed to the gradually increased HOMO energies from the Sc complex to the Mn complex.

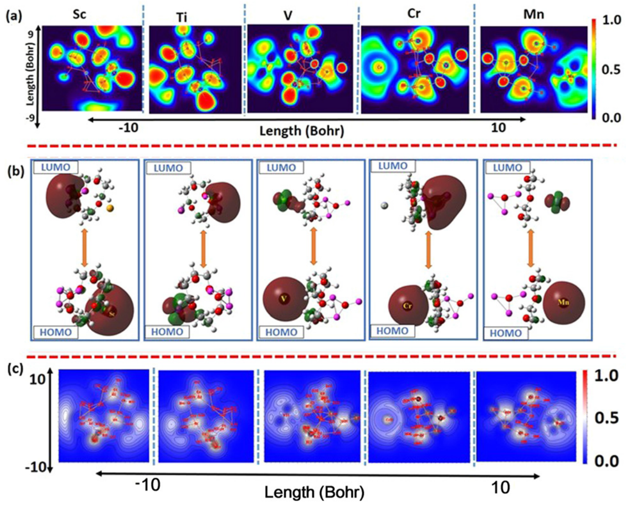

Fig. 3 The plotted (a) ELF spectra, (b) HOMO and LUMO orbitals, and (c) localized orbital locator maps of the designed Li_3O@[12-crown-4]M complexes (isovalue = 0.025) at the ωB97xd/def2tzvp level.

Fig. 3 shows the outcomes of the electron localization function (ELF) and localized orbital locator (LOL) analyses. The ELF explains the electron pair density to manifest the surface topology of complexes with high ELF values indicated by red color and blue color manifesting delocalized regions. Examining the excess electron nature reveals high electron localization around transition metals. From Fig. 3a, we can see that a strong negative charge appears on the M atom in the Sc and Ti complexes, and the intensity of the red color decreases and delocalization increases on moving from left to right (Fig. 3). This can be attributed to the growing number of unpaired electrons in the d-orbital and the repulsion between them. Additionally, the increased interaction distance results in reduced electron localization. The localized orbital locator (LOL) is also given in Fig. 3c. Mathematically, the ELF and the LOL exhibit similar chemical mapping because they depend on the kinetic energy density. ELF is a dimensionless quantity, in the range of 0–1, to provide a visual description of the chemical bond in the present complexes. The ELF includes the Pauli kinetic energy density, while the LOL analysis does not include Pauli repulsion. The LOL further unveils the excess electron localization in d-orbitals of M in the present complexes. In addition, VIP and VEA values are computed for the present complexes, as shown in Table 2. The reduced VIP values suggest an increased tendency for electron donation, enhancing interactions among complex fragments. Notably, these values are considerably lower than those of individual Li_3O and [12-crown-4]. Interestingly, the VIP values of these complexes are also lower than those of alkali metals. In fact, the VIP values for Sc, Ti, V, and Cr complexes are even smaller than the ionization potential of caesium (3.89 eV), the lowest among all elements. Readily electron loosing tendency of present complexes also indicates the formation of more stable anionic species. This can also be correlated with the potential interaction and stability of metalide complexes. For instance, VIP values of present complexes are significantly lower than those reported for coinage metalides $M–F_6C_6H_6–M$ (where M = Cu, Ag, and Au),[11] M′–$F_6C_6H_6$–M (where M′ = Li, Na, and K, and M = transition metals),[20] and M–Janus–M (where M = Sc–Zn).[21] In these metalides, the ns^1 electrons of alkali metals are polarized and transferred to transition metals (M′), where negative NBO charges are observed on transition metals. Consequently, the present metalide complexes based on superalkali are intriguing candidates for further exploration of their NLO properties.

3.3 Static nonlinear optical properties

It is evident that the present Li_3O@[12-crown-4]M (where M = Sc, Ti, V, Cr, and Mn) complexes display strong metalide character and can be included in the excess electron compound family. Literature also justifies the dramatic role of excess electrons in molecular materials in enhancing static and dynamic NLO features.[21,22,55–57] The present superalkali-based metalides show better NLO responses over conventional metalides. The computed polarizability (α_o), hyperpolarizability (β_o), and projection of hyperpolarizability on the dipole moment (β_{vec}) vector are given in Table 3. A remarkable enhancement is observed in the static α_o values of complexes as compared to pristine [12-crown-4], and values range from 4.3×10^2 to 4.1×10^2 a.u. The α_o of the Sc complex is the highest among other series of the present complexes. The components of α_o and β_o are also plotted in Fig. 4. The increased α_o values of complexes suggest their linear optical response and the significant effect of the external electric field.

The nonlinear optical effect is estimated through the calculated static first hyperpolarizability (β_o) values, ranging from 7.6×10^5 to 1.7×10^4 a.u., where the highest value is observed for the Sc complex (also see Fig. 5a). The remarkable β_o value of the Sc complex is 12 622 times higher than that of pristine [12-crown-4] (see Table 3). The significant NLO response of the Sc complex may be attributed to the strong metalide character and the reduced VIP value. Similarly, the presence of excess electrons decisively decreases the excitation energy ΔE (2.76 eV) of the Sc complex. The remaining Ti, V, Cr, and Mn complexes have β_o values of 5.9×10^4, 8.3×10^3, 7.9×10^3, and 1.7×10^4 a.u., respectively. The β_o value monotonically decreases from Sc to Cr, while the Mn complex shows a slightly higher response. The rising trend of β_o can be linked to the electronic properties such as VIP, HOMO–LUMO gaps, metalide character, and the nuclear charge on M. Complexes with strong metalide character, reduced VIP, and low excitation energies, resulting in excellent NLO features. In α_o, the α_x component is dominant, but β_z contributes significantly to the total hyperpolarizability response. Furthermore, values of projection of hyperpolarizability on dipole moment (β_{vec}) are also given in Table 3. The results of β_{vec} are consistent with those of β_o, which confirms that the designed metalides are remarkable NLO materials.

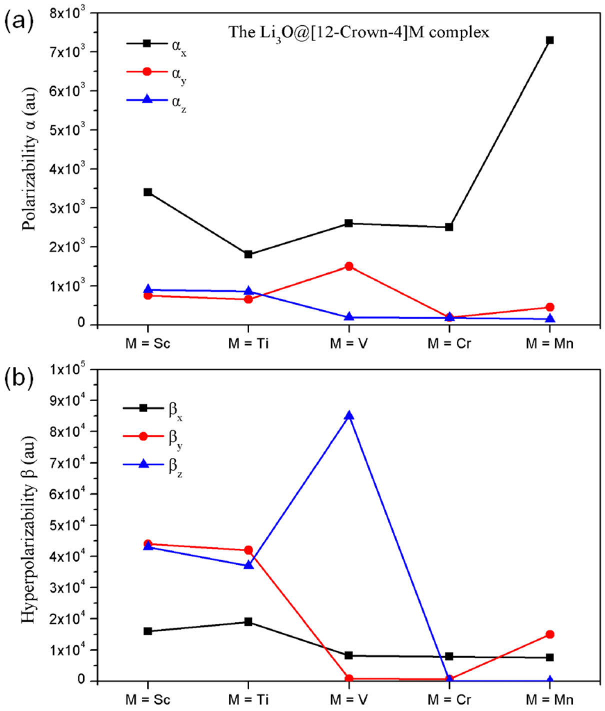

Fig. 4 Components of NLO properties: (a) polarizability (α_o) and (b) hyperpolarizability (β_o) of the Li_3O@[12-crown-4]M (where M = Sc, Ti, V, Cr, and Mn) complexes using the ωB97xd/def2tzvp method.

Table 4 lists the static second hyperpolarizability (γ_o), which is the third-rank NLO response for molecular materials, and the average contribution to hyperpolarizability. The γ_o value of [12-crown-4] is 9.9×10^3 a.u., while the values dramatically increase up to 5.6×10^6 a.u. for the V complex. The significant γ_o response of the V complex might be attributed to its noticeable μ_o and reduced E_g. Overall, the γ_o values range from 1.7×10^5 to 5.6×10^6 a.u., demonstrating excellent third-order NLO properties. A comparison of the NLO properties is made with reported metalides and transition metals containing simple excess electron compounds. The exceptional NLO features of current metalides reveal why they are chosen over traditional alkalides and simple excess electron complexes. In the present study, β_o of the Sc complex is higher than those of coinage

Table 3 Static polarizabilities α_o (in a.u.), static first hyperpolarizabilities β_o (in a.u.), components of hyperpolarizability, and projection of hyperpolarizabilities on dipole moment vectors β_{vec} (in a.u.) of the studied complexes

Complexes	α_o	α_x	α_y	α_z	β_o	β_x	β_y	β_z	β_{vec}
[12-crown-4]	1.0×10^2	1.1×10^2	1.1×10^2	8.7×10^1	60.21	1.2×10^{-2}	6.0×10^2	60.01	60.02
Li_3O@[12-crown-4]Sc	4.3×10^2	3.4×10^3	7.5×10^2	9.0×10^2	7.6×10^5	1.6×10^4	4.4×10^4	4.3×10^4	6.2×10^3
Li_3O@[12-crown-4]Ti	4.2×10^2	1.8×10^3	6.5×10^2	8.6×10^2	5.9×10^4	1.9×10^4	4.2×10^4	3.7×10^4	3.6×10^3
Li_3O@[12-crown-4]V	2.0×10^2	2.6×10^3	1.5×10^3	1.9×10^2	8.3×10^3	8.2×10^3	8.2×10^2	8.5×10^2	8.5×10^2
Li_3O@[12-crown-4]Cr	2.0×10^2	2.5×10^3	1.9×10^2	1.8×10^2	7.9×10^3	7.9×10^3	6.5×10^2	1.6×10^2	7.9×10^3
Li_3O@[12-crown-4]Mn	4.1×10^2	7.3×10^1	4.5×10^2	1.5×10^2	1.7×10^4	7.6×10^3	1.5×10^4	7.0×10^1	8.2×10^3

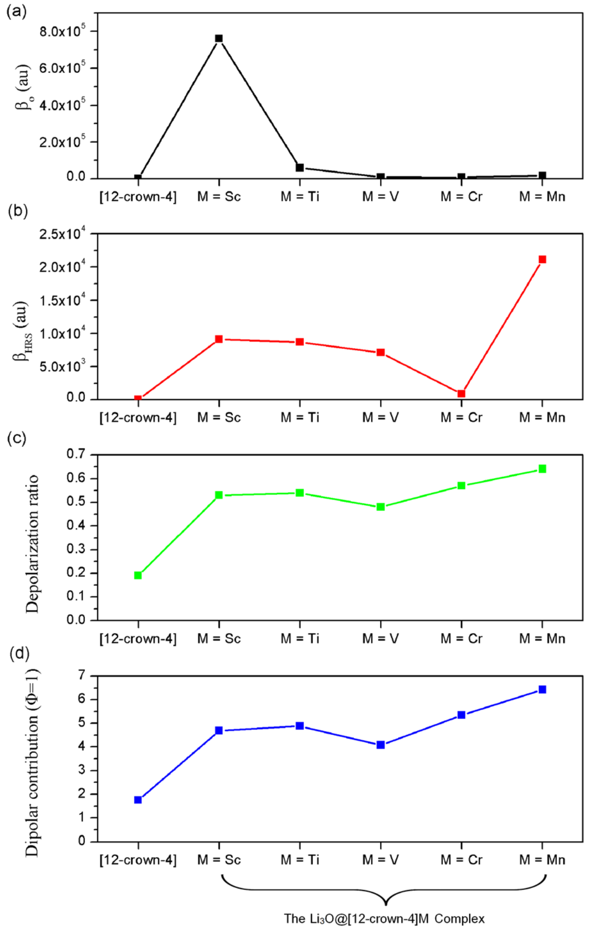

Fig. 5 Plotted static (a) first hyperpolarizability (β_o), (b) hyper-Rayleigh scattering first hyperpolarizability (β_{HRS}), (c) depolarization ratio, and (d) dipolar contribution to hyperpolarizability $\Phi(\beta_{j=1})$ of the studied complexes at the ωB97xd/def2tzvp level.

metalides[19] and transition metal-based Janus metalides.[21] Likewise, the unprecedented involvement of Li_3O in regulating vdW forces and charge transfer also makes them interesting candidates over single metal-based alkalides and metalides. The involvement of vdW forces and charge transfer to transition metals render them appealing competitors over single metal-based alkalides and metalides for NLO applications.[58,59]

The effect of solvent on the NLO properties was investigated at the ωB97xd/def2tzvp level. An implicit solvent effect using the universal solvent based on solute electron density (SMD) is considered,[60] and the results are reported in Table S3. In the implicit solvent effect, water with a dielectric constant of 78.35 exhibits a slightly higher β_o response as compared to ethanol, but Cr and Mn complexes hold significant β_o values in ethanol (see Fig. 6). Overall, entire complexes show a better hyperpolarizability response in the solvent medium as compared to the gas phase. The enhancement in β_o is attributed to structural changes in complexes influenced by solvent polarity. In water and ethanol, an excellent increase in the dipole moment is recorded, influencing the hyperpolarizability response. Hence, strong polarization effects and charge fluctuations are key parameters in enhancing the static NLO properties using the SDM model.

The calculated hyper-Rayleigh scattering first hyperpolarizability (β_{HRS}) and its components are also given in Table 4 and Fig. 5b. β_{HRS} is a parametric optical effect that occurs when two incoming photons of frequency ω annihilate, resulting in a scattered photon of frequency 2ω. A substantial enhancement of the β_{HRS} is seen for the designed metalides as compared to the pristine complexant. β_{HRS} values range from 8.4×10^2 to 2.1×10^4 a.u., where the Mn complex holds the highest value of scattering and the first hyperpolarizability among the series. The highest value for the Mn complex might be credited to its significant dipole moment and lowest HOMO–LUMO gap (E_g). In addition, the β_{HRS} response could be related to the d^5 electron system and delocalization of electrons in the Mn complex. The significant dipolar contribution percentage might be a contributing factor for the increased β_{HRS} of the Mn complex. Unlike previous studies on similar systems, the present complexes show no correlation between the dipole moment and β_{HRS}.[61–63] However, a correlation exists between E_g and the dipole moment in the studied complexes. As the interaction distance between the metal (M) and the oxygen/hydrogen atoms of [12-crown-4] increases, the value of E_g gradually decreases. Concurrently, the dipole moment follows an increasing trend from Sc to Mn complexes. The values of $\langle\beta_{j=1}\rangle$ and $\langle\beta_{j=3}\rangle$ are also higher for the Mn complex. From Fig. 5d, an increased dipolar contribution to hyperpolarizability $\Phi(\beta_{j=1})$ can be observed with the depolarization ratio (DR), suggesting the dipolar nature of complexes.

The NLO response of complexes can be separated into dipolar $\Phi(\beta_{j=1})$ and octupolar $\Phi(\beta_{j=3})$ contributions to total hyperpolarizability,[59] and the contribution percentages to hyperpolarizability are given in Table 4. The $\Phi(\beta_{j=1})$ dipole characteristics prevail in cases where charge transfer and

Table 4 Static second hyperpolarizabilities γ (in a.u.), projection of hyperpolarizability on dipole moment vector β_{HRS} (in a.u.), average dipolar hyperpolarizability $\langle\beta_{j=1}\rangle$ (in a.u.), average octupolar hyperpolarizabilities $\langle\beta_{j=3}\rangle$ (in a.u.), dipolar contribution percentage to hyperpolarizability $\Phi(\beta_{j=1})$, octupolar contribution percentage to hyperpolarizability $\Phi(\beta_{j=3})$, and depolarization ratio of the present complexes

Complexes	γ_o	β_{HRS}	$\langle\beta_{j=1}\rangle$	$\langle\beta_{j=3}\rangle$	$\Phi(\beta_{j=1})$	$\Phi(\beta_{j=3})$	DR
[12-crown-4]	9.9×10^3	46.33	34.13	1.4×10^2	0.19%	0.80%	1.75
Li_3O@[12-crown-4]Sc	5.7×10^5	9.1×10^3	1.6×10^4	1.4×10^4	0.53%	0.47%	4.69
Li_3O@[12-crown-4]Ti	9.6×10^5	8.7×10^3	1.6×10^4	1.3×10^4	0.54%	0.45%	4.88
Li_3O@[12-crown-4]V	5.6×10^6	7.1×10^3	1.2×10^4	1.3×10^4	0.48%	0.51%	4.02
Li_3O@[12-crown-4]Cr	1.7×10^5	8.4×10^2	1.6×10^3	1.2×10^3	0.57%	0.42%	5.34
Li_3O@[12-crown-4]Mn	4.7×10^6	2.1×10^4	4.2×10^4	2.3×10^4	0.64%	0.35%	6.42

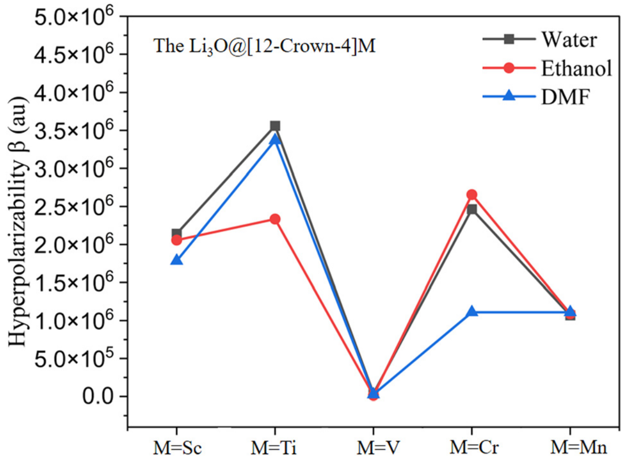

Fig. 6 The plotted hyperpolarizability (β_o) with implicit solvents at the ωB97xd/def2tzvp/SMD (water, ethanol, and DMF) level.

dipole moment are almost one-dimensional. The pure [12-crown-4] ether has an octupolar nature as revealed by significant octupolar contribution percentage with $\Phi(\beta_{J=3}) \approx 79\%$ to total hyperpolarizability. In contrast, a notable dipolar contribution to hyperpolarizability is observed in Li_3O@[12-crown-4]M complexes, signifying their dipolar nature. Furthermore, the dipolar nature of complexes can also be observed from their computed depolarization ratio (DR). In particular, a small DR value of 1.75 is calculated for the pure complexant, which evidences its octupolar nature, while the designed complexes reflect high DR values. The DR values oscillate between 1.5 (octupolar) and 9 (dipolar). For the present metalides, the DR value is between 4.02 and 6.42, confirming the dipolar nature of these complexes.

3.4 Dynamic NLO response and metalide character

To obtain a comprehensive understanding of NLO characteristics, we have estimated the frequency-dependent NLO parameters. The frequency-dependent first hyperpolarizability $\beta(\omega)$ parameters are calculated for electro-optical Pockel's effect (EOPE) with $\beta(-\omega;\omega,0)$ and electric field-induced second harmonic generation (ESHG) with $\beta(-2\omega;\omega,\omega)$ at applied frequencies of 532, 1064, 1300, and 1500 nm, respectively. From Table 5, it can be found that the $\beta(\omega)$ responses are much higher than the corresponding static hyperpolarizability (β_o). The larger the externally applied frequency, the greater the $\beta(\omega)$ value. One can notice the reduced frequency-dependent $\beta(\omega)$ at an applied frequency of 1500 nm. Similarly, the EOPE effect and ESHG are more responsive at a higher dispersion frequency of 532 nm. The highest value of EOPE (5.0×10^9 a.u.) is obtained for the Mn complex, while the lowest value of 6.3×10^3 a.u. is observed for the Cr complex at 1500 nm. Overall, the order is EOPE (at 532 nm) > EOPE (at 1064 nm) > EOPE (at 1300 nm) > EOPE (at 1500 nm). Among the present complexes, the Mn complex possesses remarkable values for the frequency-dependent hyperpolarizability response.

Likewise, frequency-dependent second hyperpolarizability $\gamma(\omega)$ values are also provided in Table 5. Overall, the values of $\gamma(\omega)$ are quite higher than the corresponding static ones, indicating the influence of externally applied frequencies on the NLO features. In the series, the Ti and Cr complexes exhibit extraordinary responses for $\gamma(\omega)$. $\gamma(-\omega;\omega,0,0)$ is determined for the dc-Kerr effect, and $\gamma(-2\omega;\omega,\omega,0)$ is determined for the second harmonic generation (SHG) effect.[64] The complexes exhibit better dynamic NLO responses at higher dispersion frequency, and the dc-Kerr effect becomes less intense at 1500 nm except for the Cr complex. The dc-Kerr effect is the effect of an instantaneously occurring nonlinear response and plays a crucial role in photonics and optoelectronics. The Cr complex is more responsive at the applied frequency of 1500 nm. Entire metalides show a higher dynamic $\gamma(\omega)$ response at high external frequencies. For these complexes, the dc-Kerr effect is distinct at a small applied frequency (532 nm)

Table 5 Frequency-dependent dynamic first hyperpolarizability with electro-optic Pockel's effect (EOPE) $\beta(-\omega;\omega,0)$, electric field-induced second harmonic generation (ESHG) $\beta(-2\omega;\omega,\omega)$, the frequency dependent second hyperpolarizability for Kerr effect $\gamma(-\omega;\omega,0,0)$ and SHG $\gamma(-2\omega;\omega,\omega,0)$ response with ω = 0.085, 0.042, 0.035, and 0.030 a.u. for the studied complexes

Frequency		[12-crown-4]	Li_3O@[12-crown-4]Sc	Li_3O@[12-crown-4]Ti	Li_3O@[12-crown-4]V	Li_3O@[12-crown-4]Cr	Li_3O@[12-crown-4]Mn
Frequency-dependent first hyperpolarizability $\beta(\omega)$ (a.u.)							
0.085 (532 nm)	$\beta(-\omega;\omega,0)$	49.32	1.5×10^5	5.0×10^5	1.5×10^5	6.0×10^4	2.6×10^5
	$\beta(-2\omega;\omega,\omega)$	64.23	9.8×10^4	3.6×10^4	9.8×10^4	1.8×10^5	2.6×10^4
0.042 (1064 nm)	$\beta(-\omega;\omega,0)$	49.10	1.2×10^5	1.2×10^5	5.5×10^3	4.6×10^3	1.4×10^5
	$\beta(-2\omega;\omega,\omega)$	48.21	1.9×10^5	2.2×10^5	1.1×10^4	4.4×10^3	1.1×10^5
0.035 (1300 nm)	$\beta(-\omega;\omega,0)$	46.46	2.0×10^5	2.2×10^5	2.9×10^5	9.4×10^3	2.5×10^4
	$\beta(-2\omega;\omega,\omega)$	47.46	1.3×10^6	9.9×10^6	1.3×10^6	1.7×10^5	1.6×10^5
0.030 (1500 nm)	$\beta(-\omega;\omega,0)$	46.34	7.5×10^4	6.4×10^4	7.1×10^4	2.5×10^3	3.2×10^5
	$\beta(-2\omega;\omega,\omega)$	47.08	7.0×10^4	8.4×10^4	8.1×10^4	4.9×10^3	1.3×10^5
Frequency-dependent second hyperpolarizability $\gamma(\omega)$ (a.u.)							
0.085 (532 nm)	$\gamma(-\omega;\omega,0,0)$	1.0×10^4	7.7×10^8	3.1×10^{10}	7.9×10^9	8.6×10^7	8.0×10^9
	$\gamma(-2\omega;\omega,\omega,0)$	1.6×10^4	7.7×10^7	1.6×10^{10}	6.5×10^7	1.1×10^8	4.5×10^8
0.042 (1064 nm)	$\gamma(-\omega;\omega,0,0)$	1.0×10^4	1.0×10^4	6.6×10^7	3.9×10^6	1.3×10^7	2.1×10^7
	$\gamma(-2\omega;\omega,\omega,0)$	1.1×10^4	1.1×10^4	8.3×10^8	1.9×10^7	1.9×10^6	3.2×10^8
0.035 (1300 nm)	$\gamma\ (-\omega;\omega,0,0)$	4.3×10^4	9.2×10^6	1.0×10^7	2.6×10^6	2.0×10^{11}	1.8×10^7
	$\gamma(-2\omega;\omega,\omega,0)$	4.5×10^4	1.6×10^7	2.4×10^7	1.0×10^7	1.4×10^{10}	1.4×10^7
0.030 (1500 nm)	$\gamma\ (-\omega;\omega,0,0)$	4.3×10^4	2.3×10^6	3.9×10^6	3.3×10^7	2.3×10^{11}	4.5×10^6
	$\gamma(-2\omega;\omega,\omega,0)$	4.4×10^4	5.5×10^8	2.5×10^8	7.7×10^5	5.0×10^9	1.0×10^7

as compared to the 1064 nm frequency. Notably, the Mn complex exhibits the highest value of 3.1 × 10^{10} a.u. for the dc-Kerr effect, while the Cr complex holds the lowest response. In addition, quantitative analysis at 1500 nm reveals an inverse correlation between the VIP and $\gamma(-\omega;\omega,0,0)$. A systematic decrease in VIP from Sc to Mn complexes generally corresponds to enhanced $\gamma(-\omega;\omega,0,0)$ responses, with the exception of Mn complexes showing a minor reduction. Notably, the trend in γ responses contrasts with the decreasing metalide character across the series.

3.5 The role of vdW forces and NLO features

The nature of bonds among Li_3O, [12-crown-4], and M has been thoroughly examined using the quantum theory of atoms in molecules (QTAIM) analysis. The molecular pictures representing bonding critical points (BCPs) at selected electron densities (3, −1) are given in Fig. S3c. Describing covalent and non-covalent bonding forces in the present complexes, several electronic parameters such as total electron density (ρ_b), Laplacian of electron density ($\nabla^2\rho$), potential energy density (V_b), kinetic energy density (G_b), and total energy density (H_b) are evaluated. For clarity, the ring critical point (RCP) at (3, +1) and the nuclear critical point (NCP) are omitted. The topological parameters are listed in Table S4. The Laplacian of electron density ($\nabla^2\rho$) and total energy density (H_b) between M and H-atoms of [12-crown-4] are positive, suggesting that vdW forces are being operational in stabilizing complexes. As shown in Fig. 7, the intermolecular interactions in all complexes except Li_3O@[12-crown-4]Cr are formed between the oxygen atom of the Li_3O and the H-atom of the complexant. The type of interaction can be determined by examining the ratio of G_b to $|-V_b|$. If this ratio exceeds unity, it suggests a non-covalent interaction, indicating that the forces between the atoms are primarily governed by weak repulsion or attraction. If the ratio is between 0.5 and 1, it confirms the presence of electrostatic interactions between M and [12-crown-4]. As can be seen, the investigated complexes exhibit closed-shell interactions between the M and oxygen atoms of the Li_3O@[12-crown-4] complex by the positive values of H_b and $\nabla^2\rho_b$, suggesting relatively stable interactions. These interactions are predominantly non-covalent, as confirmed by the $G_b|/|-V_b|$ values exceeding unity for the majority of attractions. Moreover, the interactions between Li and oxygen atoms are also not through sharing electrons, as shown by $G_b|/|-V_b|$ values greater than 1. In contrast, the interactions of M with hydrogen atoms are dominated by electrostatic character due to $G_b|/|-V_b|$ values between 0.5 and 1. The values of H_b are negative for these interactions, while positive values of G_b are observed.

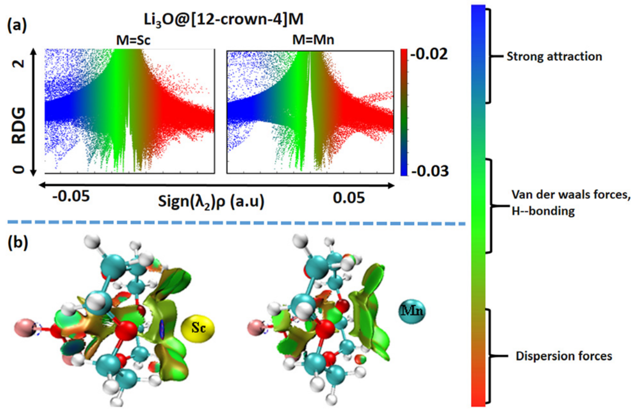

Fig. 7 The representation of intermolecular interactions. (a) The reduced density gradient (RDG) scattered plots between RDG and sign(λ_2)ρ (a.u.) and (b) isosurfaces of the Li_3O@[12-crown-4]M (where M = Sc and Mn) at the ωB97xd/def2tzvp level.

To further identify vdW forces and their important roles in electronic and NLO properties, the noncovalent interaction (NCI) analysis is considered. The RDG *versus* sign(λ_2)ρ scattered plots and the colour-filled RDG isosurface for Sc and Mn are shown in Fig. 7, while the remaining pictures are shown in Fig. S3. It can be seen from Fig. 7a that the RDG isosurface of Li_3O@[12-crown-4]M complexes holds green-coloured layered patches, suggesting vdW interactions. Moreover, the appearance of more spike blue regions in the Sc complex signifies the stronger attraction between the Sc atom and [12-crown-4], which is in agreement with the short interaction distance. The observed significant vdW interactions in the Sc complex can be attributed to its shorter interaction distance ($d_{M\text{–}H}$) and considerable NBO charge transfer, resulting in a noteworthy hyperpolarizability response. It can also be observed that the ionic pairing Li_3O^+–M^- is predominantly dominated by attractive interactions followed by vdW forces. The impact of vdW interaction is highly observed for M lying exactly in the middle of [12-crown-4]. This is reasonable because the charge transferred from Li_3O to M is significant, resulting in increased stability for the guest–host system as well as the NLO response of complexes.

The second-order perturbation energy (E^2) is also examined to gain a better comprehension of donor–acceptor orbital interactions and their contribution to the stability of the Li_3O@[12-crown-4]M complexes. Table S5 lists the corresponding results, detailing intermolecular charge transfers and electron delocalization. The E^2 is used to measure the amount of electron delocalization between the donor (i) and acceptor (j) interacting orbitals as described in eqn (15). In the present complexes, the interaction between lone pair (LP) electrons of the oxygen atom of Li_3O (donor) and LP* orbitals of M (acceptor) is the most significant donor–acceptor interaction. This delocalization of electrons in Li_3O plays a crucial role in maintaining the polar environment and its charge-donating ability to metals. Therefore, a significant E^2 value indicates a strong interaction existing between the donor and acceptor orbitals, resulting in notable stability of complexes. From the results collected in Table S5, it can be found the lowest E^2 value (0.06 kcal mol^{-1}) obtained for the Mn complex displays that it has the minimum stabilization energy for charge transfer, while a significant value (31.45 kcal mol^{-1}) is calculated for the Sc complex, demonstrating strong donor–acceptor interactions in this complex. These results are consistent with the calculated NBO charge analysis as well as with the interaction energy of the Sc complex. It should be noted that E^2 is not the sole factor enhancing NLO responses. The magnitude of E^2 is strongly dependent on both the orbital overlap and the energy difference between the donor and acceptor orbitals at specific interaction distances.

3.6 Excited state and vibrational study

Excited state analysis using the TD-DFT-ωB97xd method provides insights into the absorbance wavelengths ($\lambda_{\max}$) and vertical excitation energies (ΔE). The role of vertical excitation energy and absorbance wavelength is important for adequately understanding the nonlinear optical features of molecules and clusters. It has been reported that low excitation energy facilitates the promotion of excess electrons to unoccupied molecular orbitals, especially the lowest unoccupied molecular orbitals (LUMOs), which enhances the nonlinear optical properties of the material.[65–67] Numerical findings are presented in Table 6. The absorbance spectrum of pristine [12-crown-4] shows adsorption in the UV region with a maximum wavelength ($\lambda_{\max}$) of 127.71 nm and the corresponding excitation energy of 9.70 eV. In contrast, entire designed complexes are transparent in the UV region and exhibit absorbance at greater wavelengths (Fig. S4). The Li_3O@[12-crown-4]M complexes show absorption maxima ranging from 335.75 to 447.84 nm. The Sc complex holds the highest absorption wavelength ($\lambda_{\max}$ = 447.84 nm), while the Mn complex has the minimum ($\lambda_{\max}$ = 335.75 nm). Furthermore, the transition energies (ΔE) of Li_3O@[12-crown-4]M are monitored in the range of 2.76–3.69 eV. The designed complexes have low excitation energies as compared to [12-crown-4], while the corresponding oscillation strength values increase. In the present complexes, the excitation energy is inversely related to hyperpolarizability, as already discussed. In the Sc complex, the major contribution of orbitals is 34% and 30% for HOMO → LUMO+3 and HOMO → LUMO, respectively. Similarly, HOMO → LUMO+2 (37%) is the dominant vertical transition in the Ti complex, while HOMO → LUMO+6 (68%) is observed in the V complex.

In the gas phase, vibrational modes associated with the pristine crown-ether and the designed Li_3O@[12-crown-4]M complexes have been investigated. The FT-IR spectra of [12-crown-4] and the Li_3O@[12-crown-4]M complexes are presented in Fig. S5, while their vibrational frequencies are listed in Table S6. ν_{C-H} stretching modes in [12-crown-4] are observed in the range of 3073–2976 cm^{-1} in FT-IR spectra, closely matching the experimental values of 2947–2865 cm^{-1}.[68–70] Furthermore, three vibrations associated with ν_{C-H} bending modes, with the calculated intensities of 1496, 1401, and 1134 cm^{-1} are also in agreement with experimental results.[69] Characteristic peaks associated with crown ethers are C–O and C–C stretching. Strong peaks observed at 1227 cm^{-1} are associated with C–O stretching, while the medium peak at 1075 cm^{-1} belongs to C–C stretching. The calculated vibrational frequencies for the designed complexes correspond to stretching and bending vibrations in the range of 3029–1270 cm^{-1}. The highest C–H stretching and bending for the Cr complex are observed at 3029 cm^{-1} and 1270 cm^{-1}, respectively. Additionally, the calculated C–O stretching modes for Sc, Ti, V, Cr, and Mn are 1203, 1207, 1216, and 1323 cm^{-1}. In conclusion, after the interaction of Li_3O and transition metals with [12-crown-4], the vibrational peaks become more intense, indicating the change in the vibrational level after complexation. In the pure complexant, the C–O stretching vibration (1206 cm^{-1}) is smaller as compared to that in the designed complexes. The vibrational frequencies align in the order of Cr > V > Ti > Mn > Sc. The obtained values are 1068, 1069, 1072, 1093, and 1067 cm^{-1}, which are consistent with the experimental results.[67,68]

Furthermore, to better understand the electronic properties of the Li_3O@[12-crown-4]M complexes and orbital contributions concerning energy, the projected density of state (PDOS), as well as total density of state (TDOS) spectra, are plotted and given in Fig. S6 and S7. PDOS provides us with information about the number of states concerning energy. The energy in the PDOS plot spreads from −21 to 5.44 eV. A significant shift to high energy in the HOMO can be observed compared to [12-crown-4]. Newly generated HOMOs are observed after the interaction of Li_3O and M with the complexant. Degenerated states are higher in energy and have a contribution from the d-orbital from transition metals. A reduction in the HOMO–LUMO gap is witnessed for complexes, promoting electron transfer from occupied to unoccupied orbitals, which leads to imparting optical NLO characteristics.

Table 6 Excitation energies (ΔE), maximum absorbance wavelength ($\lambda_{\max}$), oscillator strength (f_o), mean dipole moments (μ_o), and major orbital contribution in the excited state analysis

Complexes	ΔE (eV)	f_o (a.u.)	$\lambda_{\max}$ (nm)	Major orbital contribution
[12-crown-4]	9.70	0.2273	128	HOMO → LUMO+6 (24.5%) HOMO → LUMO+5 (12.5%)
Li_3O@[12-crown-4]Sc	2.76	2.7685	447	HOMO → LUMO (30%) HOMO → LUMO+3 (34%) HOMO → LUMO+2 (9%)
Li_3O@[12-crown-4]Ti	3.00	0.3283	411	HOMO → LUMO+2 (37%) HOMO → LUMO+3 (24%) HOMO → LUMO+5 (18%)
Li_3O@[12-crown-4]V	3.07	0.4554	402	HOMO → LUMO+6 (68%) HOMO → LUMO+7 (24%)
Li_3O@[12-crown-4]Cr	3.57	0.2543	346	HOMO → LUMO+6 (10%) HOMO → LUMO+8 (11%)
Li_3O@[12-crown-4]Mn	3.69	0.3312	335	HOMO → LUMO+6 (16%) HOMO → LUMO+8 (22%)

4 Conclusions

In summary, the metalide complexes explored here contain unprecedented involvement of Li_3O as a source of excess electrons, while transition metals exhibit negative charges (anions). The existence of ion-paired species Li_3O^+@[12-crown-4]M^- (where M = Sc, Ti, V, Cr, and Mn) is very crucial in elaborating the metalide nature and vdW forces at long-range distances between Li_3O and M. Extensive electronic structure calculations unveil their excess electron nature and thermodynamic features. The artificial bee colony algorithm predicts the molecular geometries of the present complexes. The dynamic and kinetic stability of the complexes is confirmed through AIMD simulations at 300 K. Both ELF and LOL topological analyses support the metalide characteristics and provide evidence on excess electron localization to transition metals in the present complexes. A remarkable hyperpolarizability (β_o) value of 7.6×10^5 a.u. is obtained for the Sc complex, while hyper-Rayleigh scattering (β_{HRS}) is the highest for the Mn complex. With the help of excess electrons and metalide character, these complexes exhibit excellent dynamic NLO properties. The dipolar nature of the complexes is witnessed with increased atomic number and spin multiplicity. For the Sc, Ti, and Mn complexes, considerable vdW forces and attractive interactions enhance the stability as well as dynamic NLO features of the complexes. Frequency-dependent NLO responses are evaluated at 532, 1064, 1300, and 1500 nm, revealing that $\beta(\omega)$ is more prominent at 1300 nm, while $\gamma(\omega)$ exhibits high magnitude at the higher frequency (532 nm). The influence of different solvents on hyperpolarizability is evaluated using an implicit solvation model. The β_o responses with implicit solvents have a substantial increase compared to gas-phase calculations, with water yielding slightly higher β_o values. Although the present calculations employed an implicit solvent model, directional solvation effects arising from protic solvents could potentially influence the computed properties, which deserve further investigation.

Author contributions

The manuscript was written through contributions from all authors. All authors have given approval to the final version of the manuscript.

Conflicts of interest

The authors declare no competing financial interest.

Data availability

The data that support the findings of this study are available from the corresponding author upon reasonable request.

Supplementary information available: Optimized molecular geometries, snapshot of geometries in AIMD calculations, RDG scattered plots, absorption spectra, IR spectra, PDOS and TDOS spectra, the computed interaction energies, optimized geometric coordinates, static NLO parameters, topological parameters, and vibrational frequencies of the studied complexes. See DOI: **https://doi.org/10.1039/d5nj00827a**

Acknowledgements

This work was supported by the National Natural Science Foundation of China (No. 22320102004 and 22133003) and the Beijing National Laboratory for Molecular Sciences. A. A. also acknowledges the ANSO for support.

References

1 R. L. Zhong, H. L. Xu, Z. R. Li and Z. M. Su, Role of excess electrons in nonlinear optical response, *J. Phys. Chem. Lett.*, 2015, **6**, 612–619.
2 D. T. Elg, H. E. Delgado, D. C. Martin, R. M. Sankaran, P. Rumbach, D. M. Bartels and D. B. Go, Recent advances in understanding the role of solvated electrons at the plasma-liquid interface of solution-based gas discharges, *Spectrochim. Acta, Part B*, 2021, **186**, 106307.
3 S. K. Yadav, S. Bhunia, R. Kumar, R. Seth and A. Singh, Designing Excess Electron Compounds by Substituting Alkali Metals to a Small and Versatile Tetracyclic Framework: A Theoretical Perspective, *ACS Omega*, 2023, **8**, 7978–7988.
4 G. E. Gibson and W. L. Argo, The Absorption Spectra Of The Blue Solutions Of Certain Alkali And Alkaline Earth Metals In Liquid Ammonia And In Methylamine, *J. Am. Chem. Soc.*, 1918, **40**, 1327–1361.
5 A. Ellaboudy, J. L. Dye and P. B. Smith, Cesium 18-Crown-6 Compounds. A Crystalline Ceside and a Crystalline Electride, *J. Am. Chem. Soc.*, 1983, **10**, 6490.
6 X. Chen and Y. Bu, Single- versus Multi-Proton-Coupled Rydberg-State Electron Transfer in Amine Clusters, *J. Phys. Chem. C*, 2014, **118**, 18861.
7 F. Ullah, N. Kosar, K. Ayub and T. Mahmood, Superalkalis as a source of diffuse excess electrons in newly designed inorganic electrides with remarkable nonlinear response and deep ultraviolet transparency: A DFT study, *Appl. Surf. Sci.*, 2019, **483**, 1118–1128.
8 M. Cai, M. P. Miao, Y. Liang, Z. Jiang, Z. Y. Liu, W. H. Zhang, X. Liao, L. F. Zhu, D. West, S. Zhang and Y. S. Fu, Manipulating single excess electrons in monolayer transition metal dihalide, *Nat. Commun.*, 2023, **14**, 1–9.
9 R.-L. Zhong, H.-L. Xu, S.-L. Sun, Y.-Q. Qiu and Z.-M. Su, The Excess Electron in a Boron Nitride Nanotube: Pyramidal NBO Charge Distribution and Remarkable First Hyperpolarizability, *Chem. – Eur. J.*, 2012, **18**, 11350.
10 A. F. Borghesani and M. Santini, Density and Field Dependence of Excess Electron Mobility in High-Density Noble Gases BT, in *Linking the Gaseous and Condensed Phases of Matter: The Behavior of Slow Electrons*, ed., L. G. Christophorou, E. Illenberger and W. F. Schmidt, Springer US, Boston, MA, 1994, pp. 259–279.
11 X.-H. Li, X. Cheng, W.-L. Wang, D. Yu, B.-L. Ni and W.-M. Sun, Alkali-Metal-Free Coinage Metalides: Specific Pairing and Location of Doping Atoms Bring Forth High Stability

and Considerable Nonlinear Optical Response, *Organometallics*, 2022, **41**, 3697–3705.

12 R. Riedel, A. G. Seel, D. Malko, D. P. Miller, B. T. Sperling, H. Choi, T. F. Headen, E. Zurek, A. Porch, A. Kucernak, N. C. Pyper, P. P. Edwards and A. G. M. Barrett, Superalkali-Alkalide Interactions and Ion Pairing in Low-Polarity Solvents, *J. Am. Chem. Soc.*, 2021, **143**, 3934–3943.

13 X.-H. Li, X. Cheng, W.-L. Wang, D. Yu, B.-L. Ni and W.-M. Sun, Alkali-Metal-Free Coinage Metalides: Specific Pairing and Location of Doping Atoms Bring Forth High Stability and Considerable Nonlinear Optical Response, *Organometallics*, 2022, **41**, 3697–3705.

14 S. Gao, W. Li, J. Dai, Q. Wang and Z. Suo, Effect of transition metals doping on electronic structure and optical properties of β-Ga_2O_3, *Mater. Res. Express*, 2021, **8**, 025904.

15 B. Champagne, A. Plaquet, J.-L. Pozzo, V. Rodriguez and F. Castet, Nonlinear Optical Molecular Switches as Selective Cation Sensors, *J. Am. Chem. Soc.*, 2012, **134**, 8101.

16 S. Bai, D. Wang, H. Liu and Y. Wang, Recent advances of oxyfluorides for nonlinear optical applications, *Inorg. Chem. Front.*, 2021, **8**, 1637–1654.

17 S. Muhammad, Symmetric vs. asymmetric: Which one is the better molecular configuration for achieving robust NLO response, *J. Mol. Graphics Modell.*, 2022, **114**, 108209.

18 X. Chen and K. M. Ok, Metal oxyhalides: an emerging family of nonlinear optical materials, *Chem. Sci.*, 2022, **13**, 3942–3956.

19 X. H. Li, X. L. Zhang, Q. H. Chen, L. Zhang, J. H. Chen, D. Wu, W. M. Sun and Z. R. Li, Coinage Metalides: a New Class of Excess Electron Compounds with High Stability and Large Nonlinear Optical Responses, *Phys. Chem. Chem. Phys.*, 2020, **22**, 8476.

20 F. Ahsan and K. Ayub, Transition metalides based on facially polarized all-*cis*-1,2,3,4,5,6-hexafluorocyclohexane – a new class of high performance second order nonlinear optical materials, *Phys. Chem. Chem. Phys.*, 2023, **25**, 4732–4742.

21 A. Ahsin, A. Ali and K. Ayub, Transition metals based metalides TM-Janus-TM (where TM = Sc–Zn and Janus = $F_6C_6H_6$); A theoretical study of nonconventional metalides with excellent static and dynamic nonlinear optical properties, *Mater. Sci. Semicond. Process.*, 2023, **162**, 107506.

22 A. Ahsin and K. Ayub, Superalkali-based alkalides Li_3O@[12-crown-4]M (where M = Li, Na, and K) with remarkable static and dynamic NLO properties; A DFT study, *Mater. Sci. Semicond. Process.*, 2022, **138**, 106254.

23 E. Rehm, R. S. Paul von and A. I. Boldyrev, Ab Initio Study of Superalkalis. First Ionization Potentials and Thermodynamic Stability, *Inorg. Chem.*, 1992, **31**, 4834–4842.

24 R. Pal, A. Poddar and P. K. Chattaraj, Atomic Clusters: Structure, Reactivity, Bonding, and Dynamics, *Front. Chem.*, 2021, **9**, 1–24.

25 J. L. Dye, Compounds of Alkali Metal Anions, *Angew. Chem., Int. Ed. Engl.*, 1979, **18**, 587–598.

26 J. L. Dye, Electrides: Early Examples of Quantum Confinement, *Acc. Chem. Res.*, 2009, **42**, 1564–1572.

27 G. W. Gokel, W. M. Leevy and M. E. Weber, Crown ethers: Sensors for ions and molecular scaffolds for materials and biological models, *Chem. Rev.*, 2004, **10**, 2723–2750.

28 A. Nandy, C. Duan, M. G. Taylor, F. Liu, A. H. Steeves and H. J. Kulik, Computational Discovery of Transition-metal Complexes: From High-throughput Screening to Machine Learning, *Chem. Rev.*, 2021, **121**, 9927–10000.

29 W. M. Sun, L. T. Fan, Y. Li, J. Y. Liu, D. Wu and Z. R. Li, On the Potential Application of Superalkali Clusters in Designing Novel Alkalides with Large Nonlinear Optical Properties, *Inorg. Chem.*, 2014, **53**, 6170.

30 J. Cao, F. Li, W. Xia and W. Bian, van der Waals interactions in bimolecular reactions, *Chin. J. Chem. Phys.*, 2019, **32**, 157–166.

31 Z. Shen, H. Ma, C. Zhang, M. Fu, Y. Wu, W. Bian and J. Cao, Dynamical Importance of van der Waals Saddle and Excited Potential Surface in $C(^1D) + D_2$ Complex-Forming Reaction, *Nat. Commun.*, 2017, **8**, 14094.

32 D. Skouteris, D. E. Manolopoulos, W. Bian, H. J. Werner, L. H. Lai and K. Liu, van der Waals interactions in the Cl + HD reaction, *Science*, 1999, **286**, 1713–1716.

33 Q. Lu and W. Bian, The Decay of Dispersion Interaction and Its Remarkable Effects on the Kinetics of Activation Reactions Involving Alkyl Chains, *J. Phys. Chem. Lett.*, 2023, **14**, 10642–10647.

34 X. Yang, H. Ma, Q. Lu and W. Bian, Efficient Method for Numerical Calculations of Molecular Vibrational Frequencies by Exploiting Sparseness of Hessian Matrix, *J. Phys. Chem. A*, 2024, **128**, 3024–3032.

35 W. Bian and H.-J. Werner, Global ab initio potential energy surfaces for the ClH_2 reactive system, *J. Chem. Phys.*, 2000, **112**, 220–229.

36 M. J. Frisch, G. W. Trucks, H. B. Schlegel, G. E. Scuseria, M. A. Robb, J. R. Cheeseman, G. Scalmani, V. Barone, G. A. Petersson, H. Nakatsuji, X. Li, M. Caricato, A. V. Marenich, J. Bloino, B. G. Janesko, R. Gomperts, B. Mennucci, H. P. Hratchian, J. V. Ortiz, A. F. Izmaylov, J. L. Sonnenberg, D. Williams-Young, F. Ding, F. Lipparini, F. Egidi, J. Goings, B. Peng, A. Petrone, T. Henderson, D. Ranasinghe, V. G. Zakrzewski, J. Gao, N. Rega, G. Zheng, W. Liang, M. Hada, M. Ehara, K. Toyota, R. Fukuda, J. Hasegawa, M. Ishida, T. Nakajima, Y. Honda, O. Kitao, H. Nakai, T. Vreven, K. Throssell, J. A. Montgomery Jr., J. E. Peralta, F. Ogliaro, M. J. Bearpark, J. J. Heyd, E. N. Brothers, K. N. Kudin, V. N. Staroverov, T. A. Keith, R. Kobayashi, J. Normand, K. Raghavachari, A. P. Rendell, J. C. Burant, S. S. Iyengar, J. Tomasi, M. Cossi, J. M. Millam, M. Klene, C. Adamo, R. Cammi, J. W. Ochterski, R. L. Martin, K. Morokuma, O. Farkas, J. B. Foresman and D. J. Fox, *G16_C01 Gaussian 16, Revision C.01*, Gaussian, Inc., Wallingford, 2016.

37 F. Neese, F. Wennmohs, U. Becker and C. Riplinger, The ORCA quantum chemistry program package, *J. Chem. Phys.*, 2020, **152**, 224108.

38 J. Cao, Y. Wu and W. Bian, Ring polymer molecular dynamics of the $C(^1D) + H_2$ reaction on the most recent potential energy surfaces, *Chin. J. Chem. Phys.*, 2021, **34**, 833–842.

39 Y. Ren and W. Bian, Mode-Specific Tunneling Splittings for a Sequential Double-Hydrogen Transfer Case: An Accurate Quantum Mechanical Scheme, *J. Phys. Chem. Lett.*, 2015, **6**, 1824–1829.

40 F. Li, X. Yang, X. Liu, J. Cao and W. Bian, An Ab Initio Neural Network Potential Energy Surface for the Dimer of Formic Acid and Further Quantum Tunneling Dynamics, *ACS Omega*, 2023, **8**, 17296–17303.

41 J. Luo, J. Cao, H. Liu and W. Bian, Accurate quantum dynamics of the simplest isomerization system involving double-H transfer, *Chin. J. Chem. Phys.*, 2022, **35**, 185–192.

42 W. Xia, J. Cao, Q. Lu and W. Bian, Production of ultracold polyatomic molecules with strong polarity by laser cooling: A detailed theoretical study on CaNC and SrNC, *Front. Chem.*, 2022, **10**, 1009986.

43 J. Zhang and M. Dolg, ABCluster: the artificial bee colony algorithm for cluster global optimization, *Phys. Chem. Chem. Phys.*, 2015, **17**, 24173–24181.

44 J. Zhang and M. Dolg, Global optimization of clusters of rigid molecules using the artificial bee colony algorithm, *Phys. Chem. Chem. Phys.*, 2016, **18**, 3003–3010.

45 S. F. Boys and F. Bernardi, The Calculation of Small Molecular Interactions by the Differences of Separate Total Energies. Some Procedures with Reduced Errors, *Mol. Phys.*, 2006, **19**, 553–566.

46 D. Zheng and F. Wang, Performing Molecular Dynamics Simulations and Computing Hydration Free Energies on the B3LYP-D3(BJ) Potential Energy Surface with Adaptive Force Matching: A Benchmark Study with Seven Alcohols and One Amine, *ACS Phys. Chem. Au*, 2021, **1**, 14–24.

47 A. L. Tenderholt and K. M. Langner, cclib: A library for package independent computational chemistry algorithms, *J. Comput. Chem.*, 2008, **29**, 839–845.

48 T. Lu and F. Chen, Multiwfn: A multifunctional wavefunction analyzer, *J. Comput. Chem.*, 2012, **33**, 580–592.

49 W. Humphrey, A. Dalke and K. Schulten, VMD: Visual molecular dynamics, *J. Mol. Graphics*, 1996, **14**, 33.

50 K. Yokoyama, H. Tanaka and H. Kudo, Structure of Hyperlithiated Li_3O and Evidence for Electronomers, *J. Phys. Chem. A*, 2001, **105**, 4312–4315.

51 Y. Wu, J. Cao, H. Ma, C. Zhang, W. Bian, D. Nunez-Reyes and K. M. Hickson, Conical intersection–regulated intermediates in bimolecular reactions: Insights from $C(^1D)$ + HD dynamics, *Sci. Adv.*, 2019, **5**, eaaw0446.

52 J. Cao, Z. Zhang, C. Zhang, K. Liu, M. Wang and W. Bian, Quasiclassical trajectory study of H + SiH_4 reactions in full-dimensionality reveals atomic-level mechanisms, *Proc. Natl. Acad. Sci. U. S. A.*, 2009, **106**, 13180–13185.

53 F. Li, X. Liu, H. Ma and W. Bian, A diabatization method based upon integrating the diabatic potential gradient difference, *Phys. Chem. Chem. Phys.*, 2024, **26**, 16477–16487.

54 F. Li, X. Liu, X. Yang, J. Cao and W. Bian, Quantum Dynamics Calculations on Isotope Effects of Hydrogen Transfer Isomerization in Formic Acid Dimer, *Chin. J. Chem. Phys.*, 2023, **36**, 545–552.

55 R.-L. Zhong, H.-L. Xu, Z.-R. Li and Z.-M. Su, Role of Excess Electrons in Nonlinear Optical Response, *J. Phys. Chem. Lett.*, 2015, **6**, 612–619.

56 A. Ahsin and K. Ayub, Theoretical Investigation of Superalkali Clusters M_2OCN and M_2NCO (where M = Li, Na, K) as Excess Electron System with Significant Static and Dynamic Nonlinear optical response, *Optik*, 2021, **277**, 166037.

57 A. Ahsin, A. Qamar, Q. Lu and W. Bian, Theoretically designed M@diaza[2.2.2]cryptand complexes: the role of non-covalent interactions in promoting NLO properties of organic electrides, *Sci. Technol. Adv. Mater.*, 2024, **25**, 2357064.

58 A. Ahsin, A. Qamar, S. Muthu, V. Vetrivelan, J. Cao and W. Bian, Superalkali nature of the Si_9M_5 (M = Li, Na, and K) Zintl clusters: a theoretical study on electronic structure and dynamic nonlinear optical properties, *RSC Adv.*, 2024, **14**, 17091–17101.

59 A. Ahsin, T. Jadoon and K. Ayub, M@[12-crown-4] and M@[15-crown-5] where (M = Li, Na, and K); the very first examples of non-conventional one alkali metal-containing alkalides with remarkable static and dynamic NLO response, *Phys. E*, 2022, **140**, 115170.

60 A. V. Marenich, C. J. Cramer and D. G. Truhlar, Universal Solvation Model Based on Solute Electron Density and on a Continuum Model of the Solvent Defined by the Bulk Dielectric Constant and Atomic Surface Tensions, *J. Phys. Chem. B*, 2009, **113**, 6378–6396.

61 R. Bano, K. Ayub, T. Mahmood, M. Arshad, A. Sharif, A. L. Khan, H. AlMohamadi, M. Yasin and M. A. Gilani, *RSC Adv.*, 2025, **15**, 6147–6161.

62 J. Yaqoob, H. AlMohamadi, A. L. Khan, M. Yasin, T. Mahmood, K. Ayub, F. Anwar, K. S. Joya and M. A. Gilani, *RSC Adv.*, 2024, **14**, 31021–31035.

63 R. Bano, K. Ayub, T. Mahmood, M. Arshad, A. Sharif, S. Tabassum and M. A. Gilani, *Dalton Trans.*, 2022, **51**, 8437–8453.

64 W. Chen, Z.-R. Li, D. Wu, Y. Li, C.-C. Sun, F. L. Gu and Y. Aoki, Nonlinear Optical Properties of Alkalides Li + (calix[4]pyrrole)M− (M = Li, Na, and K): Alkali Anion Atomic Number Dependence, *J. Am. Chem. Soc.*, 2006, **128**, 1072.

65 D. R. Kanis, M. A. Ratner and T. J. Marks, Design and Construction of Molecular Assemblies with Large Second-Order Optical Nonlinearities. Quantum Chemical Aspects, *Chem. Rev.*, 1994, **94**, 195.

66 H. Y. Sun and H. Jiang, Combined DFT and Wave Function Theory Approach to Excited States of Lanthanide Luminescent Materials: A Case Study of LaF3:Ce3+, *J. Chin. Chem. Soc.*, 2022, **70**, 604–617.

67 A. S. Pozdeev, P. Rublev, S. Scheiner and A. I. Boldyrev, Theoretical Investigation of Geometries and Bonding of Indium Hydrides in the In2Hx and In3Hy (x = 0–4,6; y = 0–5), Series, *Molecules*, 2023, **28**, 183.

68 Y. S. Kim, H. M. Lee, J. H. Kim, J. Joo and I. W. Cheong, Hydrogel adsorbents of poly(*N*-isopropylacrylamide-*co*-methacryloyloxymethyl-12-crown-4) for Li+ recovery prepared by droplet microfluidics, *RSC Adv.*, 2015, **5**, 10656–10661.

69 S. Al-Rusaese, A. A. Al-Kahtani and A. A. El-Azhary, Experimental and Theoretical Study of the Vibrational Spectra of 12-Crown-4–Alkali Metal Cation Complexes, *J. Phys. Chem. A*, 2006, **110**, 8676–8687.

70 F. L. Cook, T. C. Caruso, M. P. Byrne, C. W. Bowers, D. H. Speck and C. L. Liotta, Facile syntheses of 12-crown-4 and 15-crown-5, *Tetrahedron Lett.*, 1974, **15**, 4029–4032.